Midinfrared metamaterials fabricated by nanoimprint lithography

Wei Wu,[a] Zhaoning Yu, Shih-Yuan Wang, and R. Stanley Williams
Quantum Science Research, HP Labs, Hewlett-Packard, Palo Alto, California 94304

Yongmin Liu, Cheng Sun, and Xiang Zhang
NSF Nano scale Science and Engineering Center (NSEC), 5130 Etcheverry Hall, University of California, Berkeley, California 94720

Evgenia Kim and Y. Ron Shen
Department of Physics, University of California, Berkeley, California 94720

Nicholas X. Fang
Department of Mechanical and Industrial Engineering, University of Illinois, Urbana-Champaign, Illinois 61801

(Received 11 September 2006; accepted 6 January 2007; published online 6 February 2007)

A metamaterial comprising an ordered array of four metallic L-shaped components designed to operate in the mid-IR frequency regime has been fabricated and characterized. The fourfold rotational symmetry of the unit cell should suppress the undesirable bianisotropy observed for split-ring resonators. Nanoimprint lithography was used to demonstrate scalability for mass production. A dipole plasmon resonance with a negative permittivity and a magnetic resonance with a negative permeability were observed at wavelengths of 3.7 and 5.25 μm, respectively, in agreement with theoretical predictions. © *2007 American Institute of Physics*.
[DOI: 10.1063/1.2450651]

Negative index metamaterials (NIMs) that exhibit unique refractive and imaging properties have recently attracted worldwide research interest.[1–4] They have opened up opportunities in nanophotonics and optical integration. For example, split-ring resonators (SRRs), which provide the negative permeability required for constructing NIMs, have demonstrated working frequencies from the microwave up to the telecommunication region as the SRRs were scaled down from millimeter to nanometer size.[5–9] However, fabricating these structures with high precision, high throughput, and low cost remains challenging, especially for metamaterials operating in the infrared or visible range. Most of the previous metamaterials in this range were fabricated by electron-beam lithography (EBL),[8,9] since the feature sizes are smaller than the resolution of state-of-the-art photolithography. However, EBL has very low throughput and, consequently, is not feasible for mass production. On the other hand, nanoimprint lithography (NIL) is a parallel process, and it has the advantages of high throughput, low cost, and high resolution.[10]

In this letter, we report the first application of nanoimprint lithography to fabricate a metamaterial of an ordered array of four L-shaped resonators (LSRs), which was proposed in Ref. 11. Each resonator consists of four L-shaped metallic arms with fourfold rotational symmetry, as schematically shown in Fig. 1(a). When magnetic fluxes thread through the LSRs, the induced current circulating along the arms gives rise to an effective magnetic dipole at the resonance frequency, which is determined by the inductance (L) and capacitance (C) of the structure as $\omega_0 = 1/\sqrt{LC}$. Although the working principle of LSRs is the same as that of traditional SRRs based on *RLC* resonances, LSRs are more isotropic. Moreover, from their symmetry, LSRs are expected to suppress the bianisotropy seen for SRRs, which is undesirable for magnetic metamaterials.[12,13]

Using Microwave Studio (CST, Germany), a commercial electromagnetic mode solver based on a finite-difference time domain algorithm, we calculated the reflection and

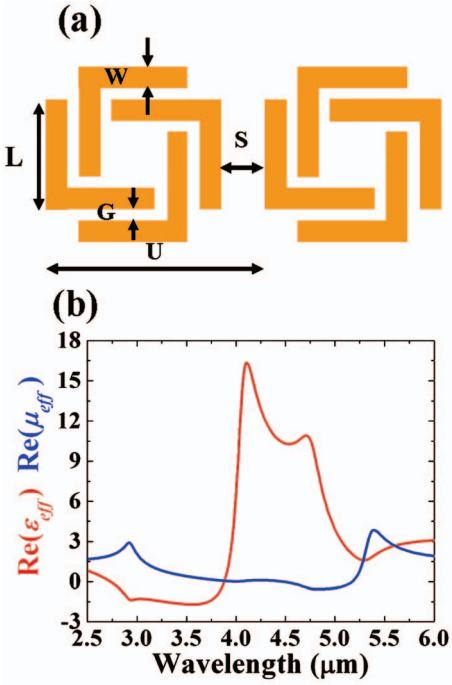

FIG. 1. (Color) (a) Schematic of L-shaped resonators (LSRs). The design parameters are arm width W=90 nm, arm length L=550 nm, gap G=45 nm, spacing S=110 nm, and lattice constant $U=L+S+2W+2G$ =930 nm. (b) Calculated effective permeability (μ_{eff}) and effective permittivity (ε_{eff}). The magnetic resonance gives rise to negative μ_{eff} from ~4.5–5.16 μm, while ε_{eff} is negative because of a pronounced electric plasmon resonance in the range of ~2.73–3.9 μm. Strong reflections should occur in these two frequency bands.

[a]Electronic mail: wei.wu@hp.com

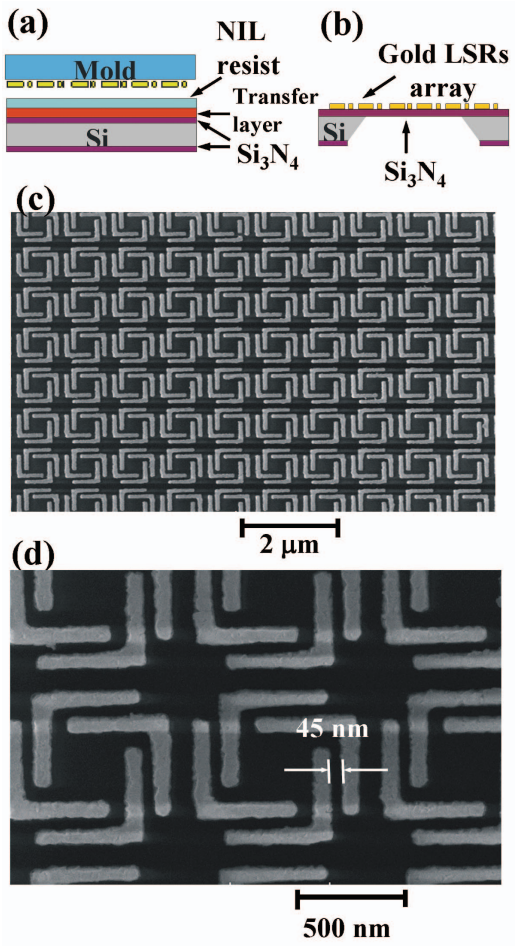

FIG. 2. (Color) (a) Illustration of the nanoimprint lithography procedure. (b) The schematic of LSRs on a Si_3N_4 membrane. (c) SEM image of a fragment of the final LSR metamaterial (total size is about 1 mm × 100 μm). (d) SEM image of LSRs demonstrating the smallest feature size of about 45 nm.

transmission coefficients for a single unit cell of an LSR, which were then used to determine the effective permittivity (ε_{eff}) and permeability (μ_{eff}) of the metamaterial.[14] As shown in Fig. 1(b), there is a clear Drude-Lorentz resonance in the μ_{eff} dispersion curve centered at 5.22 μm. Because of the strong magnetic resonance, μ_{eff} is negative over a broad band region (~4.5–5.16 μm). In addition, LSRs also possess a pronounced electric resonance, which results in a negative ε_{eff} at shorter wavelengths below 3.9 μm. Since the effective index $n_{\text{eff}}=\sqrt{\varepsilon_{\text{eff}}\mu_{\text{eff}}}$ has a large imaginary part when $\text{Re}(\varepsilon_{\text{eff}})\text{Re}(\mu_{\text{eff}})<0$, a large reflectance occurs at both the magnetic and electric resonance frequencies.

NIL was used to fabricate LSR arrays on two different substrates with plasmon and magnetic resonances designed to be in the midinfrared range. There were two major tasks in the metamaterial production: the NIL mold fabrication and the subsequent LSR array construction. The former consisted of two steps: first, fabrication of a silicon master mold using EBL and reactive ion etching (RIE); and second, duplication of the silicon mold into a transparent glass daughter mold by NIL [Fig. 2(a)] followed by lift-off and RIE. In this approach, the transparent mold was fabricated without using EBL on a nonconductive substrate, which would have degraded the resolution of the features because of the charging of the substrate. There were five steps in the array construction [Fig. 2(b)]. First, low pressure chemical vapor deposition (LPCVD) was used to deposit silicon nitride films on both sides of a standard silicon wafer. A layer of silicon oxide was thermally grown on the silicon before the LPCVD deposition to help release possible stress in the deposited nitride films. Second, a NIL transfer layer and resist were coated onto one side of the wafer and imprinted with the mold using double layer UV-curable NIL process.[15] The resulting pattern was etched into the transfer layer by RIE. Afterwards, 5 nm of Cr (to promote adhesion) and 95 nm of Au were deposited onto the patterned structure using e-beam evaporation. Third, a metal lift-off process was employed to etch away the resist and transfer materials and leave the patterned metal structure directly on the silicon nitride film. This completed the fabrication of the metal LSR array on the front side of the silicon wafer. Fourth, windows centered over the LSR arrays were patterned on the back side of the wafer using photolithography and RIE etching. Finally, a KOH anisotropic wet etch was used to remove the silicon through the back side window, and a subsequent etch with HF removed the SiO_2 layer to leave the Si_3N_4 membrane with the metal LSR array on it. Scanning electron microscopy (SEM) images of a portion of the resulting 1 mm × 100 μm metal LSR array are displayed in Fig. 2, showing a critical dimension control better than 10 nm as in Fig. 2(d). We also prepared samples that maintained the Si on the back side. This allowed us to test how the high refractive index of the Si substrate supporting the Si_3N_4 film could influence the optical properties of the two-dimensional LSR metamaterial.

To characterize the LSR arrays, we used a widely tunable optical parametric amplifier pumped by a picosecond mode-locked neodymium doped yttrium aluminum garnet laser. The output of this system had a wavelength tuning range from 2.5 to 9 μm with 20 ps pulses at a 20 Hz repetition rate. The beam could be focused down to less than 80 μm in diameter by a set of ZnSe lenses onto the LSR array. This procedure allowed a better match of the beam size on the small sample compared to characterization using Fourier transform infrared spectroscopy. In our experiment, the tunable IR beam was linearly polarized and incident on the sample at 70° with respect to the surface normal, which provided an illuminated area of about 80 × 250 μm^2, as schematically shown in Fig. 3(a). For *s*-polarization [see Fig. 1(b)], external fields could excite both the magnetic resonance and the electric plasmon resonance of the LSRs. In contrast, only the plasmon resonance could be excited for *p*-polarized light, since the magnetic field is in the plane of the LSRs. The reflected signal was detected with a thermoelectrically cooled photovoltaic detector.

Figure 3(b) shows the reflection spectrum from the LSR array on the 300 nm Si_3N_4 membrane for the *s*-polarized incident light (red squares). Two peaks are observed in the reflection spectrum. One is centered at 3.7±0.05 μm (~81 THz), resulting from the plasmon resonance due to the negative ε_{eff} of the LSRs, and the other is centered at 5.25±0.05 μm (~57 THz) due to the magnetic resonance. This result agrees with our prediction from the calculated effective parameters [see Fig. 1(b)]. As a reference, the reflection spectrum from the Si_3N_4 membrane alone was measured and plotted in Fig. 3(b) (green diamonds). It appears as a smooth background. The reflection spectrum for the *p*-polarized incident light is plotted in Fig. 3(c) (red squares), which exhibits only the plasmon resonance at 3.7±0.05 μm,

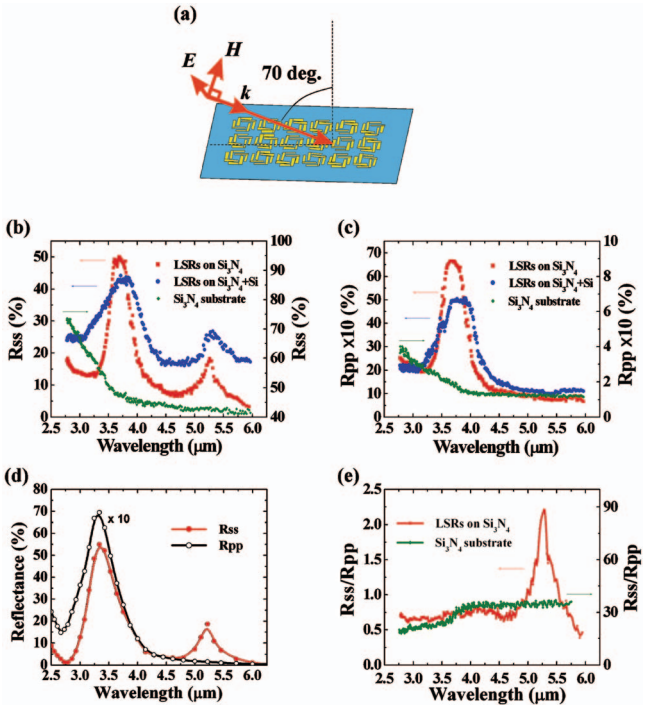

FIG. 3. (Color) (a) Illustration of the experimental configuration, in which *s*-polarized light is incident at 70° in order to excite the magnetic response of the LSR array. (b) Reflection spectra for the *s*-in and *s*-out polarization configuration for LSRs suspended on the Si_3N_4 membrane (red squares) and on the $Si+SiO_2+Si_3N_4$ substrate (blue circles), and for the Si_3N_4 membrane alone (green diamonds). (c) Reflection spectra for the *p*-in and *p*-out polarization configuration for LSRs on the Si_3N_4 membrane (red squares) and on the $Si+SiO_2+Si_3N_4$ substrate (blue circles), and for the Si_3N_4 membrane alone (green diamonds). (d) Simulated reflection spectra for LSRs on a Si_3N_4 membrane. (e) Reflection spectra with *s*-in and *s*-out polarizations normalized against *p*-in and *p*-out polarizations from nanoimprinted LSRs on a Si_3N_4 membrane (red curve) and from the Si_3N_4 membrane only (green curve).

because the in-plane magnetic field cannot excite a magnetic resonance in this case.

To confirm our interpretation of the experimental results, we calculated the reflection spectra for *s*- and *p*-polarized excitations. The results from a simulation of one LSR unit cell with a plane wave incident at 70° were used in modeling an 80×250 array using the antenna array function in Microwave Studio. The calculated reflectance spectra, which are shown in Fig. 3(d), were obtained after normalizing the far-field intensity to the incident light and agree with the experimental data [see curves in Figs. 3(b) and 3(c)].

The *s*- and *p*-polarized reflectance spectra of the same LSR array on the Si_3N_4 film supported by the Si wafer are also shown in Figs. 3(b) and 3(c) (see blue circles), respectively. Both the plasmon resonance and the magnetic resonance peaks display a redshift and a decrease of amplitude. This is the consequence of an increase of the effective refractive index of the substrate from $n\sim2$ for Si_3N_4 to $n>2$ for $Si_3N_4+SiO_2+Si$ ($n\sim3.7$ for Si). The plasmon resonance should be redshifted if the dielectric constant of the medium surrounding the metal nanostructure is increased.[16] For the magnetic resonance, the redshift occurs mainly because the larger refractive index of the substrate increases the capacitance of the LSRs. The higher effective refractive index of $Si_3N_4+SiO_2+Si$ also gives rise to a larger nonresonant background and, consequently, smaller and broader resonant peaks. In this respect, the Si_3N_4 membrane is a better substrate compared with $Si_3N_4+SiO_2+Si$.

To highlight the magnetic resonance of the LSR structure, we present in Fig. 3(e) the *s*-polarized reflection spectrum normalized against the *p*-polarized spectrum from the metamaterial on the Si_3N_4 membrane. In such a plot, the plasmon resonance is suppressed and the magnetic resonance is emphasized. As seen in Fig. 3(e), the sharp magnetic resonance peak centered at 5.25 ± 0.05 μm is clearly present. A similarly normalized spectrum for the Si_3N_4 membrane alone is relatively flat.

In summary, a metamaterial structure comprising an ordered array of LSRs has been designed and fabricated by NIL with a minimum feature size of 45 nm. Characterization of such LSR arrays on two different substrates has been carried out by infrared reflection spectroscopy using a widely tunable light source. Both the electric plasmon and magnetic resonances of the LSR metamaterial, as well as their dependence on the substrate, have been observed in the reflection spectra. The experimental results agree well with our theoretical predictions. This work demonstrates the feasibility of using the NIL technique for mass production of optical metamaterials.

One of the authors (Y.L.) thanks D. Wu for valuable discussions. The authors thank DARPA for partial support for our research.

[1]V. G. Veselago, Sov. Phys. Usp. **10**, 509 (1968).
[2]R. A. Shelby, D. R. Smith, and S. Schultz, Science **292**, 77 (2001).
[3]J. B. Pendry, Phys. Rev. Lett. **85**, 3966 (2000).
[4]N. Fang, H. Lee, C. Sun, and X. Zhang, Science **308**, 534 (2005).
[5]D. R. Smith, W. J. Padilla, D. C. Vier, S. C. Nemat-Nasser, and S. Schultz, Phys. Rev. Lett. **84**, 4184 (2000).
[6]T. J. Yen, W. J. Padilla, N. Fang, D. C. Vier, D. R. Smith, J. B. Pendry, D. N. Basov, and X. Zhang, Science **303**, 1494 (2004).
[7]S. Zhang, W. Fan, B. K. Minhas, A. Frauenglass, K. J. Malloy, and S. R. J. Brueck, Phys. Rev. Lett. **94**, 037402 (2005).
[8]S. Linden, C. Enkrich, M. Wegener, J. F. Zhou, T. Koschny, and C. M. Soukoulis, Science **306**, 5700 (2004).
[9]C. Enkrich, M. Wegener, S. Linden, S. Burger, L. Zschiedrich, F. Schmidt, J. F. Zhou, T. Koschny, and C. M. Soukoulis, Phys. Rev. Lett. **95**, 203901 (2005).
[10]S. Y. Chou, P. R. Krauss, W. Zhang, L. Guo, and L. Zhuang, J. Vac. Sci. Technol. B **15**, 2897 (1997).
[11]T. J. Yen, Ph.D. thesis, UCLA, 2005.
[12]W. J. Padilla, http://arxiv.org/PS cache/cond-mat/pdf/0508/0508307.pdf
[13]R. Marques, F. Medina, and R. Rafii-El-Idrissi, Phys. Rev. B **65**, 144440 (2002).
[14]D. R. Smith, S. Schultz, P. Markos, and C. M. Soukoulis, Phys. Rev. B **65**, 195104 (2002).
[15]W. Wu, G.-Y. Jung, D. L. Olynick, J. Straznicky, Z. Li, X. Li, D. A. A. Ohlberg, Y. Chen, S.-Y. Wang, J. A. Liddle, W. M. Tong, and R. S. Williams, Appl. Phys. A: Mater. Sci. Process. **80**, 1173 (2005).
[16]H. Raether, *Surface Plasmons* (Springer, Berlin, 1988).